

# Deeply Activated Salient Region for Instance Search

Hui-Chu Xiao  
Xiamen University  
Siming district, Xiamen, China  
hcxiao@stu.xmu.edu.cn

Wan-Lei Zhao  
Xiamen University  
Siming district, Xiamen, China  
wlzhao@xmu.edu.cn

## Abstract

*Due to the lack of suitable feature representation, effective solution to the instance search is still slow to occur. In this paper, a novel instance-level feature descriptor is proposed. The feature is built upon the salient instance region that is activated by a layer-wise back-propagation process. Such kind of region usually covers the major part an instance and represents the common patterns shared among instances of the same category. The back-propagation starts from the last convolution layer of pre-trained CNN that is originally used for classification. This makes the feature representation remain effective for instances from both known and unknown categories. Moreover, experiments show that it is effective for instance as well as image search tasks.*

## 1. Introduction

Instance search is to look for a given visual instance over a collection of images or video sequences. The query instance is usually specified by a bounding-box within an image/video frame. It is essentially different from the conventional image search task in the sense it requires the system to return the relevant images/videos along with the instance location in the images or video frames. This issue arises from several application scenarios. In the video editing task, one would like to search for all the relevant videos that a certain character or object is in presence. In the online survey, the popularity of a brand (e.g., “Coca cola”) can be roughly estimated by the frequency of a logo that appears over web images. Another wide application about instance search is seen in online shopping. In this scenario, the user is allowed to launch a query about any specific products in a given image. It could be a bag, a watch, or a hat that is worn by a person.

This issue is interesting yet challenging. First of all, most of the techniques that are proposed for content-based image retrieval are not naturally feasible for instance search. Typically, for image global features, the features from the differ-

ent instances in an image are embedded into one vector. As a consequence, one could no longer expect the feature representation is distinctive for each individual instance. With this kind of representation, the query instance is compared to the whole image instead of an instance. Moreover, the instance localization from the image is not achievable. Recent global deep features [3, 27], although powerful, face similar disadvantages.

At the time when instance search emerged as a research issue, it was addressed as a sub-image retrieval task [2]. In the typical processing framework, Bag-of-visual Word (BoVW) [33] based on hand-crafted local features such as SIFT [20] and SURF [4] is adopted [44]. Although encouraging performance is reported [2], the underlying issues of this solution can hardly overcome. On the one hand, in the most of the cases, thousands of local features are extracted from one image. These features are mostly extracted from image regions that are rich of textures or corners. As a result, textureless regions might remain uncovered. It is therefore possible that no feature representation or no sufficient representation is produced for a latent instance. On the other hand, local features are known to be invariant to geometric transformations such as scaling, rotation, and affine. However, they turn out to be vulnerable to non-rigid deformations, which are widely observed in the real scenarios.

Recently, due to the great success of convolutional neural networks (CNNs) in many computer vision tasks such as image classification [16], object detection [30], and particularly instance segmentation [7, 17], CNNs have been introduced to instance search [40]. The instance-wise vector representation is produced by ROI-pooling on each segmented instance area. Compared to the image global and local features, it is an instance-level feature and robust to object deformations. The instance search (including localization) is easily achieved by the direct comparison between the features from the query and candidate instances. Satisfactory performance is reported from [40]. However, this approach requires pixel-level annotations, which is too demanding to be feasible in many scenarios. Moreover, pixel-level annotation also makes the approach only sensitive to the known

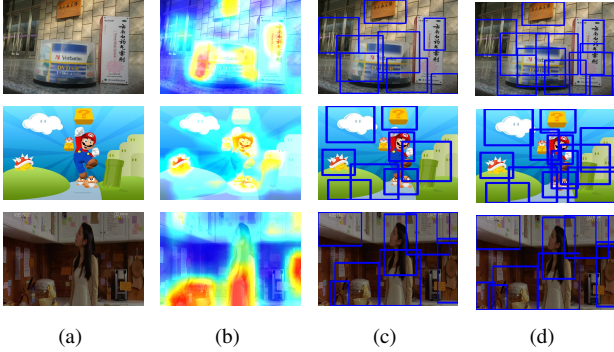


Figure 1. Localization results of three sampled images. (a) shows the original sampled images. (b) illustrates the mean activation map as heatmap overlapping on the original image for better visualization. Colors with red-tone indicate relatively high responses of common patterns, and those with blue-tone indicate low responses. (c) and (d) show the localization results without and with NMS, respectively. Best viewed in color.

categories. The latent instances from the unknown categories are ignored as the background class [7]. One faces the similar situation if we alternate to visual object detection networks [6, 30, 29] to support the instance level feature representation.

In this work, we explore the feature representation and localization for instance based on the pre-trained convolution network originally used for visual category classification. Namely, the pre-trained CNNs, e.g. ResNet are adopted to detect the potential instances in an image. In the meantime, a feature descriptor is derived from the feature map with the detected instance region. This is achieved by back-propagating the response peaks in the last convolution layer of a classification network. As we back-propagate the peak responses layer by layer, the region residing on a visual instance that supports the classification decision is activated from each layer in the network. Finally, the activated salient region is localized on the input image as the back-propagation reaches the input layer. The compact feature representation is produced by average-pooling over the corresponding region from the feature map. Both the instance-wise localization and feature representation are achieved based on only a pre-trained network. No object level or pixel-level annotations are required. It therefore relieves the burden of annotating and training thousands of instance categories. Additionally, it keeps approach to remain sensitive to instances from the unknown categories. Such kind of feature representation shows satisfactory performance on instance search. Interestingly, it also shows encouraging performance on conventional image retrieval tasks as the bag of instance-level features of one image are encoded by VLAD [13].

The remainder of this paper is organized as follows. Sec-

tion 2 reviews the state-of-the-art works in instance search and weakly supervised object detection. Our instance-level feature, namely deeply activated salient region (DASR) is presented in Section 3. The effectiveness of the proposed new feature representation is studied on the instance and image search in Section 4. Section 5 concludes the paper.

## 2. Related Work

### 2.1. Instance Search

Instance search was addressed as a sub-image retrieval task before CNNs are introduced [2] to visual object detection. Hand-crafted image local features such as SIFT [20] and SURF [4] are mainly adopted. Essentially, the relevant instances are discovered by matching the local features between the query instance and the candidate images. Due to the high computational cost of direct point-to-point matching, the encoding approaches such as BoVW [33] and VLAD [13] are introduced to speed-up the matching. There are several disadvantages in this type of approach. Firstly, conventional image local features are vulnerable to non-rigid deformations and heavy viewpoint changes, poor performance is reported when the queries are mostly non-rigid objects [40]. Moreover, local features are mostly detected along the boundaries or corners of an object. The corresponding descriptors are derived from the point regions that cover across several instances. As a result, the feature representation of a local region is actually mixed with information from different instances. Although more distinctive than the hand-crafted local features, recent deep local features [23, 24] face similar disadvantage. Furthermore, there are typically hundreds to thousands of local features are detected from one image, which is much more than the number of potential instances in one image. Given such a big number of features, on the one hand, the computation cost could be prohibitively high by point-to-point matching between the query instance and candidate images. On the other hand, the search quality is considerably degraded as we embed them with BoVW or VLAD for the sake of efficiency.

Recently, several attempts have been made to seek for instance-wise feature representation. Most of recent works rely on the fine-tuned CNNs that are designed for object detection or instance segmentation tasks. Approach in [31] utilizes an object detection framework to generate object bounding boxes from which region-level features are extracted. However, only the target instance in the top-retrieved image is located due to its high computation cost. While approach from [40] is able to generate instance-level feature representations as it is built upon fully convolutional instance-aware semantic segmentation (FCIS). Although satisfactory performance is reported from [40], the fine-tuned CNNs are only sensitive to the known instance

categories. In order to alleviate this problem, approach in [18] builds the instance-level representation based on weakly supervised object detection framework, which only requires image-level class labels. Very close performance as the fully supervised approach [40] is achieved in the paper. However, the pitfall of this approach is that the network requires extra training stage and its compatibility to the unknown categories is undermined due to the extra training.

## 2.2. Weakly Supervised Object localization

In order to produce the instance level feature representation, one critical step is to localize the instance region. Fully supervised CNN networks used for object detection or instance segmentation are unsuitable since they are insensitive to the unseen categories. Therefore, weakly supervised object detection approach which only requires image-level class annotations is preferred. Besides the proposal clustering learning (PCL) adopted in [18], there are mainly two ways to localize the object in an image based on the weakly supervised networks. One representative way follows a multiple instance learning (MIL) [21, 36, 34] pipeline. Each image is viewed as a bag consisting of several object proposals and each object proposal is viewed as an instance. During the training, MIL iteratively selects the instance with the highest confidence score. Alternatively, another way aims to localize the instance via weakly supervised instance segmentation (WSIS). Recent approach [43] leverages the instance-level visual cue inside class activation maps (CAMs) [42], which are produced by back-propagating iteratively the class-aware response peaks. The instance-level segmentation is produced by combining the activation map with the segmentation proposals. Different from above weakly supervised object localization approaches, approach in [38] only aims to mine the main object latent in one image from the last convolution layer with the high activation response. The neighboring regions with high activation responses are connected as one potential instance. The feature representation for the discovered main instance is derived from this high activation region and is used for fine-grained image retrieval. Nevertheless, this approach is unfeasible for instance search as only one instance is detected and represented in one image.

In our approach, a similar strategy as [41, 43] is adopted. Namely, the localization is based on pre-trained CNNs that are used for image classification. The instance regions are localized by identifying the regions with high response in the iteratively back-propagated activation map. However, our approach differs from the existing works in three major aspects. Firstly, our approach does not intend to localize the full range of an instance. Instead, only the instance regions with high response in the activation map are localized. One localized region only corresponds to a major region in an object that supports the network to make the decision.

It could be the face of a person, or the wheel of a car, etc. Secondly, the back-propagation starts from the last convolution layer of a network, instead of the prediction layer. This makes the localization remain sensitive to regions from the unknown instance categories. Finally, since no class-aware response is considered in our approach, no fine-tune training is involved.

## 3. Deeply Activated Instance Region Detection

As witnessed in several recent works [39, 41, 43], the classification prediction that a CNN makes is mainly based on the salient visual cues residing on the relevant visual instance. This has been originally used to interpret the behavior of a convolution neural network in [39]. Since not the whole instance contributes to the classification, it is also used to model the top-down attention of a convolution neural network [41]. Alternatively, these salient regions are combined with other visual clues to realize the instance segmentation [43]. In all these works, the salient regions are detected by back-propagating response peaks detected in the classification layer. Intuitively, these regions can be used to represent the instance on which they are located. However, only the regions from the known categories are detected as the back-propagation only considers the neurons with the high classification confidence. Therefore, such kind of way is not feasible for instance level representation. In our case, all the instances from both the known and unknown categories, as long as they are present in an image, are expected to be detected and described.

In this paper, the back-propagation is designed to start from the last convolution layer, namely the layer prior to the classification layer. The local maximums in this layer are detected and back-propagated layer-by-layer until it reaches the input layer. By this way, we interestingly discover that the salient regions from both the known categories and unknown categories are activated layer-wisely and localized on the input image. In this section, our end-to-end instance level feature extraction framework that is built upon pre-trained convolution network, is presented.

### 3.1. Activated Region Localization

Given a network  $\mathcal{N}$  is already trained on a classification task, a series of feature maps are produced as we input an image  $I$  into  $\mathcal{N}$  with a forward-pass. Given  $X \in \mathbf{R}^{W \times H \times C}$  is the feature map of the last convolution layer, the activation map is defined as the mean feature map of  $X$ , namely  $\bar{X} \in \mathbf{R}^{W \times H}$ . It is easily obtained by taking the average on  $X$  over  $C$  channels. Higher values on  $\bar{X}$  represents higher confidence score that an object region presents around that image position.

Such kind of region could be a widely observed object pattern across various training examples. These object patterns in this layer are assembled to support the decision-

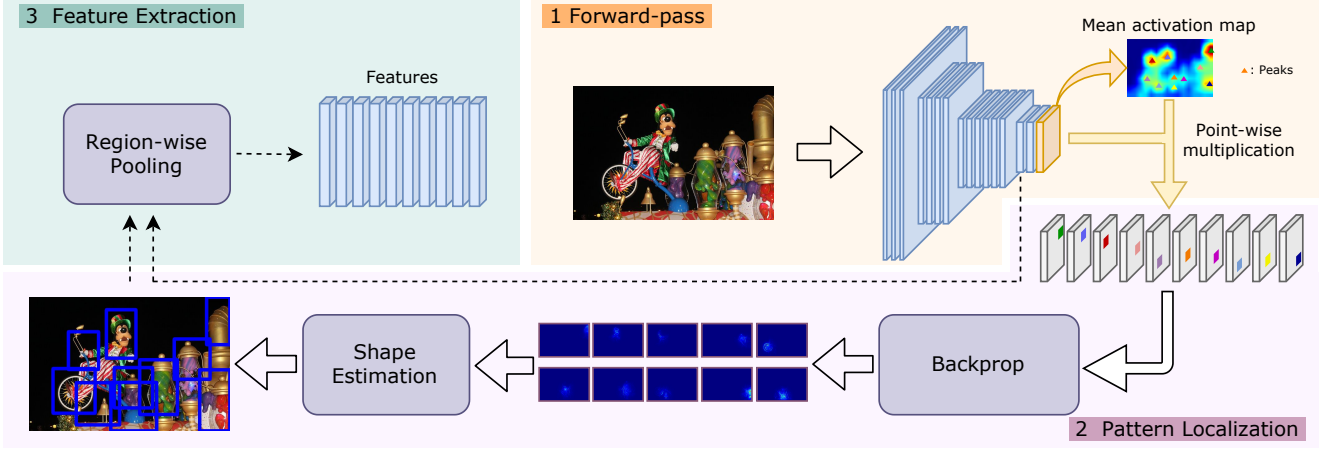


Figure 2. The pipeline of region-level features extraction based on mined common patterns. The mean activation map generated by a single forward-pass indicates the response of each position to containing common patterns. The pattern localization process further localizes each common pattern with a bounding box through a backprop and a shape estimation module. Final feature representations are built upon those localized boxes. Best viewed in color.

making in the next classification layer. Notice that  $\bar{X}$  is prior to the classification layer, even the responses from unknown categories are visible as they have not been suppressed by the classification layer. Under this observation, the local maximums are detected on  $\bar{X}$  with  $3 \times 3$  window size. These local maximums are viewed as the response peaks that network  $\mathcal{N}$  discovers from image  $I$ . They are given as set  $Q$ , in which each peak  $q$  is attached with  $x$ - $y$  position and the response value. These peaks on  $\bar{X}$  imply the most possible positions that instances might occur.

Given the position of each peak  $q \in Q$ , a probability backprop process is adopted to localize the salient region that supports to prompt the response peak in the input image. Following similar process as [41], a top-down attention model is introduced to identify task-relevant input neurons given the output responses are known.

Given no subsampling is performed in the convolution network, the convolution filter of one intermediate convolution layer is denoted as  $F \in \mathbf{R}^{W_f \times H_f \times C_{out} \times C_{in}}$ , where  $W_f \times H_f$  is the spatial size of a filter and  $C_{in}, C_{out}$  are the channel dimensions of input and output feature maps respectively. Given an image  $I$ , the input and output feature maps of this convolution layer are denoted as  $A$  and  $B$ . The activation from each spatial location in  $A$  and  $B$  could be accessed by  $A_{x,y}$  and  $B_{i,j}$  respectively. The trained weights related to  $A_{x,y}$  and  $B_{i,j}$  are accessed with  $F_{x-i,y-j}$ . The feed-forward process to generate output tensor  $B$  is formulated as

$$B_{i,j} = \sigma \left( \sum_{x=i-\frac{W_f}{2}}^{i+\frac{W_f}{2}} \sum_{y=j-\frac{H_f}{2}}^{j+\frac{H_f}{2}} F_{x-i,y-j} A_{x,y} + b \right), \quad (1)$$

where  $b$  is the bias of convolution layer and  $\sigma$  represents the

non-linear activation function.

Now let's consider to back-propagate peak pixels in the last output layer  $B$ . Notice that only the peak positions that are detected in the previous step are considered. Namely, we want to find out which positions in the input feature map  $A$  contribute to the response score in  $B_{i,j}$ , i.e.  $q$ . Following with [43, 41], this process can be modeled as a prior distribution  $P(A_{x,y})$  over output response.  $B_{i,j}$  is assumed to be the only winner which takes responses from all positions in  $A$ . Therefore, given  $P(B_{i,j})$  and  $P(A_{x,y}|B_{i,j})$  are known, we are able to work out  $P(A_{x,y})$ , viz. the probability that  $B_{i,j}$  comes from  $A_{x,y}$ .

For computational convenience,  $P(B_{i,j})$  is approximated by  $B_{i,j}$  in the last convolution layer. As a consequence, the prior probability of input  $A$  is given as

$$P(A_{x,y}) = \sum_{i=x-\frac{W_f}{2}}^{x+\frac{W_f}{2}} \sum_{j=y-\frac{H_f}{2}}^{y+\frac{H_f}{2}} P(A_{x,y}|B_{i,j})P(B_{i,j}). \quad (2)$$

In Eqn. 2, the conditional probability  $P(A_{x,y}|B_{i,j})$  is defined as

$$P(A_{x,y}|B_{i,j}) = \begin{cases} Z_{i,j} A_{x,y} F_{x-i,y-j}, & \text{if } F_{x-i,y-j} > 0 \\ 0, & \text{otherwise.} \end{cases} \quad (3)$$

where  $Z_{i,j}$  is a normalization factor to make sure that  $\sum_{i,j} P(A_{x,y}|B_{i,j}) = 1$ . The above conditional probability estimates the winning probability of position  $(x,y)$  in  $A$  given position  $(i,j)$  in  $B$  is a winning neuron. It is affected by the activation  $A_{x,y}$  and the value within convolution filter  $F_{x-i,y-j}$  which relates to  $A_{x,y}$  and  $B_{i,j}$ .

With Eqn. 2, we are able to assign a probability weight to each position in  $A$ . As we proceed the back-propagation

in the next round, the resulting  $P(A_{x,y})$  in the previous round becomes  $P(B_{i,j})$ , and  $P(A_{x,y}|B_{i,j})$  can be easily estimated in the same manner with Eqn. 3.

In addition to convolution layers, the backprop process also pass through other intermediate layers, e.g., pooling layers. The average pooling layers are regarded as performing an affine transformation on the response values of the input neurons [41]. Therefore, the average pooling layer is treated as a convolution layer that is performed within one-to-one feature map pair. For max pooling layers, error back-propagation is adopted to perform backprop in [41]. However, blanks are introduced for subsampled max pooling layers. In order to avoid such blanks, the same backprop process as convolution layer is used for max pooling layers within one-to-one feature map pair, with the weights of all-one values.

To this end, all types of layers that the back-propagation may pass through are appropriately considered with the same manner. Eqn. 2 applies to all the layers throughout the convolution network  $\mathcal{N}$ . Therefore, the back-propagation process proceeds layer by layer until it reaches the input layer. Finally, the probability that each pixel in image  $I$  contributes to a final response peak  $q$  is estimated. This leads to a probability map  $M$ , which is in the same size as image  $I$ , for one response peak  $q$ . The probabilities in  $M$  are normalized to the range  $[0, 1]$ .

Values in  $M$  indicate the degree that corresponding pixels contribute to peak  $q$ . Due to the large receptive field of the last convolution layer, pixels which do not contribute to the response peak are still assigned with low probabilities. As a result, the activated region is usually larger than it is supposed to be. A threshold  $\tau$  is introduced to filter out pixels with little contribution. In the paper,  $\tau$  is fixed to  $0.1$ . As shown in Fig. 3, such kind of pixels in general concentrate on a local region, which basically implies a potential instance in the image. With all the pixels  $r(x, y)$  in  $M$  that are greater than  $\tau$ , this activated local region is approximated by an ellipse. The parameters of the ellipse are regularized by the second moment matrix derived from all pixels  $r(x, y)$

$$\sum_{r(x,y) \geq \tau} \begin{bmatrix} x^2 & x \cdot y \\ x \cdot y & y^2 \end{bmatrix}. \quad (4)$$

Fig. 3(a) illustrates the probability maps produced from seven response peaks in one image. The corresponding shape estimation results are shown in the second row of Fig. 3. As shown in the figure, each detected region corresponds to one salient region in the image. It could cover an entire instance or a major salient region of an instance. The final localization bounding box is the circumscribed rectangle of the estimated ellipse. The feature used to describe this detected region could be derived from the corresponding area

of a feature map. Since this feature is produced by activating the salient region via a deep convolution network, it is called as *deeply activated salient region (DASR)* from now on.

### 3.2. Enhanced Instance Region Detector

In the above activation process, only the pixels with peak response in the last convolution layer are back-propagated. In practice, it is possible that more than one instance share one peak response as they are close to each other. In this case, a detected salient region will only cover one of the instances. The other neighboring instances are over-dominated. To alleviate this issue, we consider to back-propagate more number of pixels in  $\bar{X}$ . Specifically, all the pixels whose response is higher than the average value of  $\bar{X}$  are back-propagated one by one. As a result, more number of salient regions are produced. However, it is possible that two salient regions overlap with each other and cover over the same instance. In order to reduce the representation redundancy and select out the most salient regions, non-maximum suppression (NMS) is employed as [38].

The NMS is operated as follows. The intersection-over-union (IoU) threshold of NMS is given as  $\beta$ . Each candidate salient region is attached with a corresponding response value in  $\bar{X}$ . The NMS process keeps the salient region with the highest score in a local. The region is discarded as their IoUs with the already selected region are greater than  $\beta$ . The valid setting for parameter  $\beta$  is further studied in the experiment section.

With above modified detection procedure, salient regions which attain the highest response in a local are kept. While the regions from other potential instances, which have been over-dominated, could be activated as long as their overlapping with the most salient region in the local is below a threshold. On average, 11 regions are detected in one image after MNS when  $\beta$  is set to  $0.3$ . This enhanced detector is given as DASR\*. Its effectiveness is further verified in the experiment section.

### 3.3. Feature Description

**Instance level.** Once the salient regions are localized on the image, it is easy to derive feature from the feature maps. One could choose to perform either max-pooling or average-pooling over feature map within each detected region. Either way leads to a compact vector representation with uniform length. In our paper, average-pooling is selected over max-pooling for its consistently better performance. Theoretically speaking, feature map from any layer could be used to derive the feature descriptor. However, the distinctiveness varies from layer to layer. For instance, we find that feature derived from ‘‘Block4’’ in ResNet-50 shows considerably better performance over other layers across different datasets. For this reason, a standard configuration

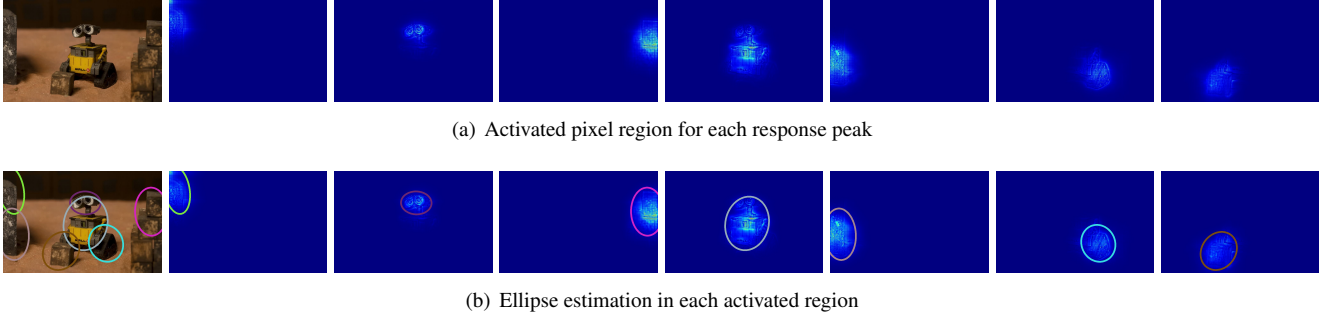


Figure 3. The illustration of deeply activated salient regions in an input image and ellipse estimation on each activated region. The first row shows the input image and activated regions with all the detected seven peaks. The corresponding estimated ellipse for each activated region is shown on the second row.

of this setting is reached after a more detailed ablation study in the experiment section. The generated features are then  $l_2$ -normalized, and undergone PCA whitening and an once more  $l_2$ -normalization.

**Image level.** One salient region basically covers one instance in an image or more usually cover a semantic part of an instance, e.g. the wheel of a car, or the face of a dog, etc. An image can be semantically viewed as a collection of instances. Similar images should share similar instances inside. It is therefore feasible to conduct similar image search with DASR. To achieve that, DASR descriptors that are extracted from each image are embedded into one vector with VLAD. Small visual word vocabulary of DASR is trained in advance. To this end, a collection of DASR features are converted into a long dense vector. Schemes proposed in VLAD\* [5] are adopted to boost the performance. As revealed in the experiment, encouraging performance is reported on image search task. It outperforms classic hand-crafted descriptor SIFT and shows competitive performance with existing deep features that are designed specifically for image search.

## 4. Experiments

### 4.1. Datasets and Experimental Setup

The proposed instance-level feature DASR is evaluated in two search tasks, namely instance search and conventional content-based image retrieval. For instance search, three evaluation benchmarks are adopted. They are Instance-160 [40], Instance-335 and INSTRE [37]. Instance-160 and Instance-335 datasets are derived from the video sequences originally used for single visual object tracking evaluation. In Instance-160, there are 160 queries and 11,885 reference images. The query instances are all covered by the 80 categories of Microsoft COCO dataset [19]. In order to test the scalability of an instance search approach, Instance-160 is augmented with 175 extra queries that are harvested from GOT-10k [10] and Youtube

BoundingBoxes [28]. Both video datasets are originally designed for object tracking evaluation. These newly added 175 query instances are out of Microsoft COCO 80 categories and the backgrounds are under severe variations. This leads to an augmented evaluation dataset Instance-335. In this dataset, there are 335 queries and 40,914 reference images. For INSTRE dataset, there are 27,293 images in total. Following with the evaluation protocol in [11], 1,250 images<sup>1</sup> are treated as the queries, leaving the remaining 27,293 images as references. For all three datasets, the bounding boxes are provided both in the query and relevant reference images.

For image retrieval task, DASR is evaluated on three popular evaluation benchmarks, namely Holidays [12], Oxford Buildings [25], and Paris [26]. In our implementation, images from above datasets are all re-sized to 512 pixels on the long side, while preserving the aspect ratio of original images. Following the convention in the literature, the search performance in two tasks is measured with mean Average Precision (mAP). For Instance-160 and Instance-335, the search performance is evaluated with varying top- $k$ , where  $k$  varies from 10 to 100. This is because the number of true-positives for each instance query varies from several to a few hundred in both Instance-160 and Instance-335.

The proposed feature extraction is actually suitable for any CNN classification network, its performance on two representative networks, namely ResNet-50 [8] and VGG-16 [32], is reported. As revealed in the later experiment, the performance from ResNet-50 is considerably higher. As a result, feature extraction with ResNet-50 is standard configuration by default. Our framework is implemented under Tensorflow framework. Experiments are run on an Nvidia GTX 1080 Ti.

In the first experiment, an ablation study is presented to investigate different layers of feature maps which is the most suitable for feature extraction. In addition,

<sup>1</sup>One instance is selected from one image.

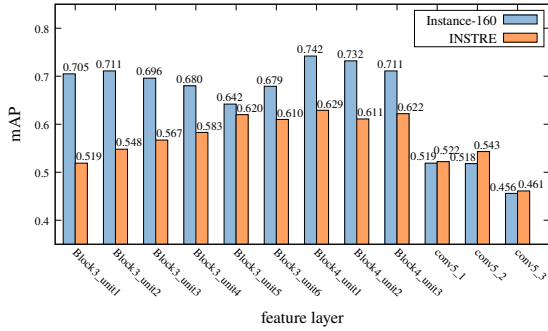


Figure 4. Performance of DASR on Instance-160 and INSTRE datasets with features derived from different convolutional layers of ResNet-50 and VGG-16.

we also study the effectiveness of adopting NMS and the valid setting for IoU rate  $\beta$  that NMS procedure involves. With the found standard configuration, the performance of DASR is studied in comparison to R-MAC [35], CroW [14], CAM [42], BLCF [22], BLCF-SalGAN [22], Regional Attention [15], DeepVision [31], FCIS+XD [40] and PCL\*+SPN [18] in the instance search task. Additionally, its performance as it is converted into a global image feature descriptor is studied in comparison to SIFT+VLAD [13], SIFT+VLAD-intra [1], R-MAC, CroW, CAM, BLCF, BLCF-SalGAN, Regional Attention and DeepVision.

## 4.2. Ablation Study

### 4.2.1 Feature Selection

Given the detected salient region, feature map from each convolutional layer could be used to derive the feature descriptor. Nevertheless, it has been widely witnessed that the search performance varies across different layers [3, 40, 18]. For this reason, ablation analysis is conducted to seek for the best suitable layer for instance search. Layers from the last two blocks of ResNet-50, namely Block3 and Block4, are investigated since deeper layers are observed to contain semantic-level information. Following the original implementation of ResNet-50, 6 and 3 bottlenecks are built within Block3 and Block4 respectively. The output feature maps from above 9 bottlenecks are respectively used to derive features for DASR region. The first bottleneck in Block3 is given as Block3\_unit1, and the rest are denoted in the same manner. For VGG-16 network, the back-propagation starts from the feature map of the 5th pooling layer, which is the last layer prior to the fully connected layers. Features are extracted from feature maps of the three convolutional layers on the 5th stage. They are given as conv5\_1, conv5\_2 and conv5\_3 respectively. In this experiment, no NMS is adopted in the region detector.

Fig. 4 shows performance on Instance-160 and INSTRE

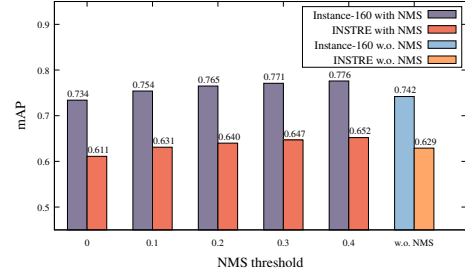


Figure 5. The performance of DASR on Instance-160 and INSTRE datasets with different NMS thresholds and without NMS.

with features output from different layers of two backbones. A wide performance gap is observed between two backbone networks. The performance gap between ResNet-50 and VGG-16 mainly comes from two perspectives, i.e., encoded patterns and feature representations. Different patterns encoded by the last convolution layer leads to different localization results. In general, the regions derived via ResNet-50 shows high localization accuracy. Moreover, feature maps from ResNet-50 are more discriminative as witnessed in many other works. Overall, features derived from Block4\_unit1 show the best performance on both datasets. As a result, it is selected as the default configuration in the rest of experiment.

### 4.2.2 Configurations on Non-Maximum-Suppression

In the second study, we further investigate the effectiveness of using NMS and the appropriate setting for overlapping rate parameter  $\beta$ . In this study, the enhanced detection procedure presented in Section 3.2 is performed on ResNet-50. Performance with different settings of  $\beta$  is presented in Fig. 5. The performance is also compared to the one without NMS. As shown in the figure, higher performance is achieved with larger overlapping rate  $\beta$ , since more salient regions are kept for one image. The highest performance is attained when  $\beta = 0.4$ , which also leads to much more number of detected regions. Namely, the number of detected regions is roughly doubled over the case of being without NMS. As a trade-off between performance and computational cost,  $\beta$  is set to 0.3 in the rest of our experiments.

With the discovered standard configuration of our feature, its effectiveness is studied in both instance and image search tasks. Specifically, the search quality, scalability as well as the localization accuracy of DASR are shown in the following sections.

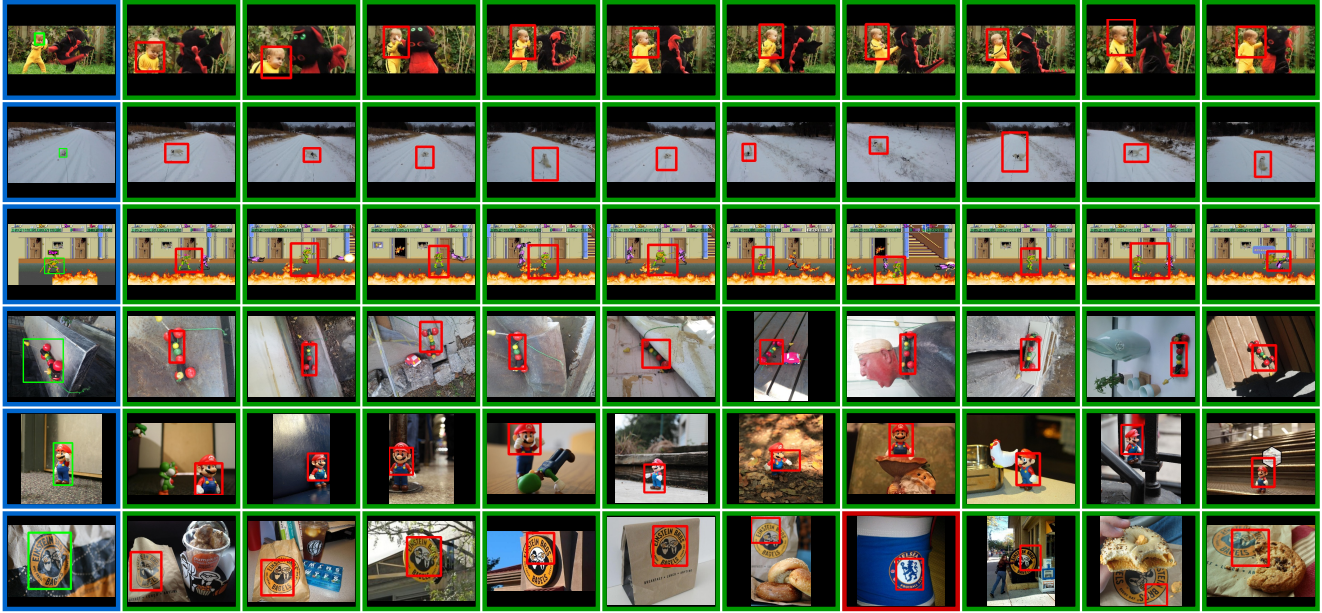


Figure 6. Top-10 retrieval results of six sample queries from Instance-335 and INSTRE. The first three rows are from Instance-335 and the last three rows are from INSTRE. Images in the first column are the queries. The following ten columns are top-10 retrieved instances along with the images where they are in presence. The returned instances are ranked by similarity score to the query. The true positives are in green border and the false positives are in red border.

### 4.3. Instance Search

#### 4.3.1 Comparison to State-of-the-Art Approaches

The performance of DASR in instance search is studied in comparison to several representative approaches in the literature. They are approaches that build upon the off-the-shelf convolutional features such as R-MAC [35], CroW [14], CAM [42], BLCF [22], BLCF-SalGAN [22] and Regional Attention [15]. Approaches that are able to produce fine-tuned region-level features such as DeepVision [31], FCIS+XD [40] and PCL\*+SPN [18] are also considered in the study. Except for DeepVision, no re-ranking or query expansion is adopted in any of the approaches.

The performance on Instance-160 and Instance-335 is shown in Tab. 1, while the performance on INSTRE is shown in Tab. 2. In general, all the approaches show steady performance degradation when they are tested on more challenging dataset Instance-335. Among all the approaches, DeepVision, FCIS+xD, PCL\*+SPN, and DASR which produce instance-level feature demonstrate better performance on both datasets. The instance-level features are more robust to background variations, which has been well-illustrated in [18]. Among these instance-level features, DASR and DASR\* show consistently satisfactory performance on both datasets. In contrast, the performance from FCIS+XD drops considerably on Instance-335 and INSTRE. It is simply because there are many instance categories outside the coverage of Microsoft COCO-80, on

Table 1. Performance comparison on Instance-160 (upper table) Instance-335 (bottom table). <sup>‡</sup> digits are cited from the referred paper

Method	Dim.	Top-10	Top-20	Top-50	Top-100	All
R-MAC [35]	512	0.101	0.164	0.268	0.307	0.358
CroW [14]	512	0.073	0.130	0.239	0.284	0.338
CAM [42]	512	0.088	0.151	0.256	0.302	0.358
BLCF [22]	336	0.131	0.247	0.487	0.592	0.653
BLCF-SalGAN [22]	336	0.137	0.255	0.493	0.596	0.656
Regional Attention [15]	2,048	0.093	0.177	0.318	0.389	0.459
DeepVision [31]	512	0.194	0.328	0.541	0.666	0.731
FCIS+XD [40] <sup>‡</sup>	1,536	<b>0.211</b>	0.356	0.575	0.659	0.724
PCL*+SPN [18]	1,024	<b>0.211</b>	<b>0.362</b>	0.583	0.661	0.724
DASR	2,048	0.204	0.348	0.591	0.680	0.742
DASR*	2,048	0.206	0.357	<b>0.614</b>	<b>0.711</b>	<b>0.771</b>
R-MAC [35]	512	0.076	0.131	0.234	0.315	0.375
CroW [14]	512	0.044	0.080	0.159	0.225	0.321
CAM [42]	512	0.059	0.104	0.194	0.263	0.347
BLCF [22]	336	0.062	0.117	0.246	0.358	0.483
BLCF-SalGAN [22]	336	0.066	0.121	0.245	0.350	0.469
Regional Attention [15]	2,048	0.059	0.119	0.242	0.351	0.488
DeepVision [31]	512	0.128	0.225	0.402	0.521	0.620
FCIS+XD [40]	1,536	<b>0.137</b>	<b>0.236</b>	0.403	0.500	0.593
PCL*+SPN [18]	1,024	0.130	0.223	0.380	0.475	0.580
DASR	2,048	0.129	0.227	0.419	0.558	0.699
DASR*	2,048	0.130	0.231	<b>0.433</b>	<b>0.580</b>	<b>0.724</b>

which FCIS+XD training fully relies. While the performance from BLCF-SalGAN fluctuates considerably across different datasets.

Top-10 retrieval results produced by our method of six sampled queries are illustrated in Fig. 6. Our method fails in some extreme cases, where the retrieved false-positive instances only differ from the query in details. As shown

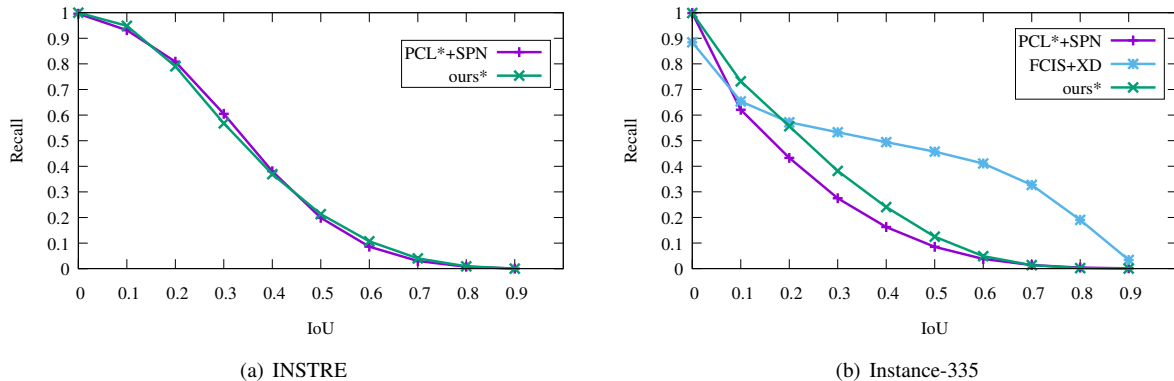


Figure 7. Recall-IoU curves on INSTRE and Instance-335. (a) compares the localization performance of PCL\*+SPN and ours on INSTRE dataset. (b) compares the localization performance of PCL\*+SPN, FCIS+XD and ours on Instance-335.

Table 2. Performance comparison on INSTRE. † digits are cited from the referred paper

Method	off-the-shelf	Dim.	All
R-MAC [35]	yes	512	0.523
CroW [14]	yes	512	0.416
CAM [42]	yes	512	0.320
BLCF [22]†	yes	336	0.636
BLCF-SalGAN [22]†	yes	336	<b>0.698</b>
Regional Attention [15]	yes	2,048	0.542
DeepVision [31]	no	512	0.197
FCIS+XD [40]	no	1,536	0.067
PCL*+SPN [18]†	no	1,024	0.575
DASR	yes	2,048	0.629
DASR*	yes	2,048	0.647

from the samples on the first two rows in Fig. 6, our approach is robust to non-rigid transformation. Furthermore, our approach is able to retrieve the instances from unseen categories. This remains true even for cartoon subjects as shown on the third row of Fig. 6. It confirms that the peak response back-propagation is able to activate the general patterns from the seen categories that are also shared by unseen categories.

### 4.3.2 Instance Localization Accuracy

In this experiment, we further study how well the detected regions overlaps with instances in the ground-truth. Following [9], recall is adopted to measure the fraction of detected regions are inside the ground-truth instances with respect to an IoU threshold. Different recalls are reported as we set IoU rate to different levels. In this experiment, only the approaches that are able to localize instance from image are considered. Namely, they are FCIS+XD, PCL\*+SPN, and DASR\*. The recall-IoU curves for three approaches produced on two datasets are shown in Fig. 7. The localization performance of FCIS+XD is not compared on INSTRE since the large portion of the instance categories are covered

in its training dataset.

As shown in the Fig. 7(a), our approach shows similar or even slightly higher performance over PCL\*+SPN, which is designed to localize the whole instance from image. While as shown in Fig. 7(b), FCIS+XD outperforms the other two approaches with large performance margin. This is not surprising since it is derived from the fully supervised segmentation network. For the reason, it is hardly to be extensible to large-scale instance search task, where hundreds to thousands of instances may occur. Compared to approach PCL\*+SPN, which is also designed to localize both known and unknown categories of instances, our approach only relies on a pre-trained CNN model without any fine-tune training.

### 4.3.3 Scalability Test

In this experiment, the scalability of DASR\* is further studied on Instance-160 by incrementally adding in one million distracting reference images. The one million distractors are crawled from Flickr. For each image, DASR\* feature is extracted with the same processing flow as before. 7,014,819 regions are detected in total by DASR\*. The scalability of DASR\* is studied in comparison to several state-of-the-art approaches ranging from conventional BoVW, BoVW+HE approaches and recent approaches, R-MAC, CroW, DeepVision and FCIS+XD. The performance from BoVW, BoVW+HE, R-MAC, and CroW is not reported above 100K scale since they are already far below the other approaches since then.

As shown in Fig. 8, DASR\* outperforms the rest of approaches across all the tested scales. Interestingly, it even outperforms FCIS+XD which are fully supervised on this dataset. The performance gap mainly comes from the feature representations. The regions detected from DASR\* are essentially salient from feature maps. As a result, the corre-

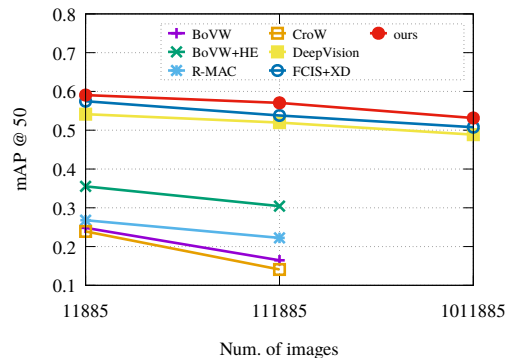


Figure 8. Scalability test on Instance-160 in comparison with several state-of-the-art methods. The performance is measured by mAP@top-50. The performance is reported as a function about the number of reference images.

sponding features are rich in pattern representations, which enhances the discriminativeness of feature representations.

#### 4.4. Image Search Performance

In this experiment, the effectiveness of DASR\* is studied when bag of DASR features from one image are converted into a global image descriptor with VLAD. In our experiment, the codebook size is fixed to 4. Unlike SIFT, it is no need to keep a large vocabulary size since there are only 7 features on average to be encoded in one image. The vocabulary is trained on an independent dataset. Following post-processing schemes proposed in [5], the resulting VLAD vectors are PCA-rotated and undergone pair-wise power-law normalization with factor 0.5.

The image search performance is studied in comparison to conventional SIFT+VLAD and various of recent approaches based on deep feature. The experiments are conducted on datasets Holidays, Oxford5k, and Paris6k. The search performance on three datasets are shown in Tab. 3. As shown in the table, it outperforms conventional approach SIFT+VLAD considerably. Most of the deep features that are specifically designed for image search show better performance over our approach. Nevertheless, the mAPs of our approach on three datasets are all above 0.6, which is sufficiently good to meet with the real search demand. More importantly, the performance of DASR on both search tasks shows that it is possible to integrate instance and image search on the same platform. It allows the user to search a specific instance in the image or search for the similar image as a whole.

## 5. Conclusion

We have presented our solution for visual instance search. The focus is on the instance-level feature represen-

Table 3. Performance comparisons on three image retrieval datasets. † digits are cited from the referred paper

Method	Dim.	Holidays	Oxford5k	Paris6k
SIFT+VLAD [13]†	4,096	0.556	0.378	-
SIFT+VLAD-intra [1]†	32,536	0.653	0.558	-
R-MAC [35]†	512	-	0.669	0.830
CroW [14]†	512	0.851	0.708	0.797
CAM [42]†	512	-	0.712	0.805
BLCF [22]†	336	-	0.722	0.746
BLCF-SalGAN [22]†	336	-	0.746	0.812
Regional Attention [15]†	2,048	-	0.768	0.875
DeepVision [31]†	512	-	0.710	0.798
DASR+VLAD	8,192	0.834	0.594	0.690

tation. A novel feature descriptor, namely DASR is proposed. The features are extracted from the semantically salient regions of an image that are activated by a back-propagation process. Both the instance localization and the corresponding feature description are performed on a classification network without any further fine-tuning. This descriptor is generic in the sense that the back-propagation could be built upon any pre-trained CNN classification network. Since no fine-tune training is required, this descriptor remains effective for the instances from both known and unknown categories, which is hardly achievable with existing approaches.

## References

- [1] Relja Arandjelovic and Andrew Zisserman. All about vlad. In *Proceedings of the IEEE conference on Computer Vision and Pattern Recognition*, pages 1578–1585, 2013.
- [2] George Awad, Wessel Kraaij, Paul Over, and Shin’ichi Satoh. Instance search retrospective with focus on TRECVID. *IJMIR*, 6(1):1–29, 2017.
- [3] Artem Babenko, Anton Slesarev, Alexandr Chigorin, and Victor Lempitsky. Neural codes for image retrieval. In *European conference on computer vision*, pages 584–599. Springer, 2014.
- [4] Herbert Bay, Tinne Tuytelaars, and Luc Van Gool. Surf: Speeded up robust features. In *European conference on computer vision*, pages 404–417. Springer, 2006.
- [5] Jonathan Delhumeau, Philippe-Henri Gosselin, Hervé Jégou, and Patrick Pérez. Revisiting the vlad image representation. In *Proceedings of the 21st ACM international conference on Multimedia*, pages 653–656, 2013.
- [6] Ross Girshick, Jeff Donahue, Trevor Darrell, and Jitendra Malik. Rich feature hierarchies for accurate object detection and semantic segmentation. In *Proceedings of the IEEE conference on computer vision and pattern recognition*, pages 580–587, 2014.
- [7] Kaiming He, Georgia Gkioxari, Piotr Dollár, and Ross Girshick. Mask R-CNN. In *Proceedings of the IEEE International Conference on Computer Vision*, pages 2961–2969, 2017.
- [8] Kaiming He, Xiangyu Zhang, Shaoqing Ren, and Jian Sun. Deep residual learning for image recognition. In *Proceed-*

- ings of the *IEEE conference on computer vision and pattern recognition*, pages 770–778, 2016.
- [9] Jan Hosang, Rodrigo Benenson, Piotr Dollár, and Bernt Schiele. What makes for effective detection proposals? *IEEE transactions on pattern analysis and machine intelligence*, 38(4):814–830, 2015.
- [10] Lianghua Huang, Xin Zhao, and Kaiqi Huang. Got-10k: A large high-diversity benchmark for generic object tracking in the wild. *arXiv preprint arXiv:1810.11981*, 2018.
- [11] Ahmet Iscen, Giorgos Tolias, Yannis Avrithis, Teddy Furon, and Ondrej Chum. Efficient diffusion on region manifolds: Recovering small objects with compact cnn representations. In *Proceedings of the IEEE Conference on Computer Vision and Pattern Recognition*, pages 2077–2086, 2017.
- [12] Herve Jegou, Matthijs Douze, and Cordelia Schmid. Hamming embedding and weak geometric consistency for large scale image search. In *European conference on computer vision*, pages 304–317. Springer, 2008.
- [13] Herve Jegou, Florent Perronnin, Matthijs Douze, Jorge Sánchez, Patrick Perez, and Cordelia Schmid. Aggregating local image descriptors into compact codes. *IEEE transactions on pattern analysis and machine intelligence*, 34(9):1704–1716, 2011.
- [14] Yannis Kalantidis, Clayton Mellina, and Simon Osindero. Cross-dimensional weighting for aggregated deep convolutional features. In *European conference on computer vision*, pages 685–701. Springer, 2016.
- [15] Jaeyoon Kim and Sung-Eui Yoon. Regional attention based deep feature for image retrieval. In *BMVC*, page 209, 2018.
- [16] Alex Krizhevsky, Ilya Sutskever, and Geoffrey E. Hinton. Imagenet classification with deep convolutional neural networks. In *Proceedings of the Advances in Neural Information Processing Systems*, pages 1097–1105, 2012.
- [17] Yi Li, Haozhi Qi, Jifeng Dai, Xiangyang Ji, and Yichen Wei. Fully convolutional instance-aware semantic segmentation. In *Proceedings of the IEEE Conference on Computer Vision and Pattern Recognition*, pages 2359–2367, 2017.
- [18] Jie Lin, Yu Zhan, and Wan-Lei Zhao. Instance search based on weakly supervised feature learning. *Neurocomputing*, 2019.
- [19] Tsung-Yi Lin, Michael Maire, Serge Belongie, James Hays, Pietro Perona, Deva Ramanan, Piotr Dollár, and C Lawrence Zitnick. Microsoft coco: Common objects in context. In *European conference on computer vision*, pages 740–755. Springer, 2014.
- [20] David G Lowe. Distinctive image features from scale-invariant keypoints. *International journal of computer vision*, 60(2):91–110, 2004.
- [21] Oded Maron and Tomás Lozano-Pérez. A framework for multiple-instance learning. In *Advances in neural information processing systems*, pages 570–576, 1998.
- [22] Eva Mohedano, Kevin McGuinness, Xavier Giró-i Nieto, and Noel E O’Connor. Saliency weighted convolutional features for instance search. In *2018 International Conference on Content-Based Multimedia Indexing (CBMI)*, pages 1–6. IEEE, 2018.
- [23] Hyeonwoo Noh, Andre Araujo, Jack Sim, Tobias Weyand, and Bohyung Han. Large-scale image retrieval with attentive deep local features. In *Proceedings of the IEEE international conference on computer vision*, pages 3456–3465, 2017.
- [24] Mattis Paulin, Matthijs Douze, Zaid Harchaoui, Julien Mairal, Florent Perronin, and Cordelia Schmid. Local convolutional features with unsupervised training for image retrieval. In *Proceedings of the IEEE international conference on computer vision*, pages 91–99, 2015.
- [25] James Philbin, Ondrej Chum, Michael Isard, Josef Sivic, and Andrew Zisserman. Object retrieval with large vocabularies and fast spatial matching. In *2007 IEEE Conference on Computer Vision and Pattern Recognition*, pages 1–8. IEEE, 2007.
- [26] James Philbin, Ondrej Chum, Michael Isard, Josef Sivic, and Andrew Zisserman. Lost in quantization: Improving particular object retrieval in large scale image databases. In *2008 IEEE conference on computer vision and pattern recognition*, pages 1–8. IEEE, 2008.
- [27] Ali Sharif Razavian, Josephine Sullivan, Atsuto Maki, and Stefan Carlsson. Visual instance retrieval with deep convolutional networks. *arXiv preprint arXiv: 1412.6574*, 2016. <https://arxiv.org/pdf/1412.6574.pdf>.
- [28] Esteban Real, Jonathon Shlens, Stefano Mazzocchi, Xin Pan, and Vincent Vanhoucke. Youtube-boundingboxes: A large high-precision human-annotated data set for object detection in video. In *Proceedings of the IEEE Conference on Computer Vision and Pattern Recognition*, pages 5296–5305, 2017.
- [29] Joseph Redmon and Ali Farhadi. Yolov3: An incremental improvement. *arXiv preprint arXiv:1804.02767*, 2018.
- [30] Shaoqing Ren, Kaiming He, Ross Girshick, and Jian Sun. Faster R-CNN: Towards real-time object detection with region proposal networks. In *Proceedings of the Advances in Neural Information Processing Systems*, pages 91–99, 2015.
- [31] Amaia Salvador, Xavier Giró-i Nieto, Ferran Marqués, and Shin’ichi Satoh. Faster r-cnn features for instance search. In *Proceedings of the IEEE Conference on Computer Vision and Pattern Recognition Workshops*, pages 9–16, 2016.
- [32] Karen Simonyan and Andrew Zisserman. Very deep convolutional networks for large-scale image recognition. *arXiv preprint arXiv:1409.1556*, 2014.
- [33] Josef Sivic and Andrew Zisserman. Video google: A text retrieval approach to object matching in videos. In *ICCV*, pages 1470–1477, 2003.
- [34] Peng Tang, Xinggang Wang, Xiang Bai, and Wenyu Liu. Multiple instance detection network with online instance classifier refinement. In *Proceedings of the IEEE Conference on Computer Vision and Pattern Recognition*, pages 2843–2851, 2017.
- [35] Giorgos Tolias, Ronan Sifre, and Hervé Jégou. Particular object retrieval with integral max-pooling of cnn activations. *arXiv preprint arXiv:1511.05879*, 2015.
- [36] Fang Wan, Chang Liu, Wei Ke, Xiangyang Ji, Jianbin Jiao, and Qixiang Ye. C-mil: Continuation multiple instance learning for weakly supervised object detection. In *Proceedings of the IEEE Conference on Computer Vision and Pattern Recognition*, pages 2199–2208, 2019.

- [37] Shuang Wang and Shuqiang Jiang. Instre: a new benchmark for instance-level object retrieval and recognition. *ACM Transactions on Multimedia Computing, Communications, and Applications (TOMM)*, 11(3):37, 2015.
- [38] Xiu-Shen Wei, Jian-Hao Luo, Jianxin Wu, and Zhi-Hua Zhou. Selective convolutional descriptor aggregation for fine-grained image retrieval. *IEEE Transactions on Image Processing*, 26(6):2868–2881, 2017.
- [39] Matthew D Zeiler and Rob Fergus. Visualizing and understanding convolutional networks. In *European conference on computer vision*, pages 818–833. Springer, 2014.
- [40] Yu Zhan and Wan-Lei Zhao. Instance search via instance level segmentation and feature representation. *arXiv preprint arXiv:1806.03576*, 2018.
- [41] Jianming Zhang, Sarah Adel Bargal, Zhe Lin, Jonathan Brandt, Xiaohui Shen, and Stan Sclaroff. Top-down neural attention by excitation backprop. *International Journal of Computer Vision*, 126(10):1084–1102, 2018.
- [42] Bolei Zhou, Aditya Khosla, Agata Lapedriza, Aude Oliva, and Antonio Torralba. Learning deep features for discriminative localization. In *Proceedings of the IEEE conference on computer vision and pattern recognition*, pages 2921–2929, 2016.
- [43] Yanzhao Zhou, Yi Zhu, Qixiang Ye, Qiang Qiu, and Jianbin Jiao. Weakly supervised instance segmentation using class peak response. In *Proceedings of the IEEE Conference on Computer Vision and Pattern Recognition*, pages 3791–3800, 2018.
- [44] Cai-Zhi Zhu and Shin’ichi Satoh. Large vocabulary quantization for searching instances from videos. In *Proceedings of the 2nd ACM International Conference on Multimedia Retrieval*, pages 1–8, 2012.